The Electron Cyclotron Absorption Diagnostic for the JET Pumped Divertor Plasma

R J Smith, D V Bartlett, A E Costley, S Richards[1].

JET Joint Undertaking, Abingdon, Oxon, OX14 3EA.
[1] Imperial College of Science, Technology and Medicine, London, SW7 2BZ.

The Electron Cyclotron Absorption Diagnostic for the JET Pumped Divertor Plasma

R.J. Smith, D.V. Bartlett, A.E. Costley and S. Richards*

JET Joint Undertaking, Abingdon Oxon OX14 3EA, UK
**Imperial College of Science, Technology and Medicine, London, SW7 2BZ, UK*

ABSTRACT

We present the design of a diagnostic system to measure electron cyclotron absorption at the second harmonic E-mode resonance in the JET pumped divertor plasma. The diagnostic will measure transmission as a function of frequency along one or more sightlines from which the spatial profile of the neTe product will be deduced. The divertor is briefly described, and the electron cyclotron resonance physics relevant to this measurement is reviewed. The problems of measuring transmission using an oversized transmission system are discussed and the chosen measurement technique, a swept frequency interferometer using a coherent radiation source, is described. A prototype of the instrument has been assembled to test the measurement technique. Some data demonstrating the instrument's characteristics are presented. The non-resonant losses, which may affect the interpretation of the measurement, are also discussed.

1 INTRODUCTION

1.1 The JET Pumped Divertor

The pumped divertor, which is presently being installed in JET, will provide a means of controlling the quantity of impurities introduced into the main plasma from the material walls [1]. Impurities sputtered from the target tiles will be entrained by, and transported by, the scrap-off layer (SOL) plasma due to frictional forces and will be pumped out of the divertor region using cryopumps. The divertor will also provide a means of density control. Deuterium gas will be injected into the private flux region of the divertor to create a cool, dense plasma that will efficiently radiate energy. In addition, the plasma strike points on the divertor target will be swept across the tiles to distribute the heat load more uniformly. In the first phase, the target tiles will be made of carbon and will be radiatively cooled. Figure 1 is a poloidal cross-section of the torus showing the divertor coils, target plates and cryopump in relation to the main plasma. A three-dimensional view of a section of the divertor is shown in Figure 2.

The electron temperature, T_e, in the divertor plasma is not expected to exceed 200 eV but the electron density, n_e, is expected to be high, around 10^{20} m^{-3}. Close to the target, the temperature will fall to perhaps a few eV and the density will increase substantially.

A number of diagnostics are currently being developed for the measurement of divertor plasma parameters. They will form an essential part of the experimental programme aimed at understanding and optimizing the performance of the divertor, as well as validating divertor

models. The microwave diagnostics contributing to this information will be a two frequency interferometer, a reflectometer detecting peak density, and the electron cyclotron absorption (ECA) diagnostic.

1.2 Choice of Diagnostic Technique

It can be seen in Figure 1 that the divertor is at about the same major radius as the plasma centre. Hence, the core plasma will radiate intensely at the same frequencies as those for which EC interactions will be a maximum in the divertor plasma. As will be shown below, even the second harmonic E-mode resonance will have low optical depth (generally <2) in the divertor. A measurement of ECE would therefore be dominated by wall reflected emission from the core plasma, and not give any information about the local T_e of the divertor plasma.

Since the divertor plasma will not be completely opaque, a transmission measurement using radiation from an external source (modulated so that it can be distinguished from the intense background of the core plasma) will be possible. Such a measurement of electron cyclotron absorption (ECA) should provide a spatially localized determination of the optical depth which, for a tenuous plasma, is directly related to the local n_eT_e product, or the local electron pressure. In combination with other divertor diagnostics which measure n_e, it should be possible to obtain spatial profiles of T_e.

Figure 3 shows the expected operating space for the divertor plasma on an n_e vs T_e diagram, with electron cyclotron transmissivity levels of 0.1 and 0.9 for the second harmonic E-mode, and assuming an on-axis toroidal magnetic field of 3.0 tesla. For this figure the finite density effects have been neglected. This is discussed further in Section 2.1. It can be seen that the expected range of n_e and T_e values is well covered by an ECA diagnostic which can measure transmission between 0.1 and 0.9.

2 ECA THEORY

Although a number of ECA measurements have been made on tokamaks [2,3], and they have shown broad agreement with the predictions of theory, electron cyclotron absorption has not been used before as a routine diagnostic. We therefore give a brief review of the electron cyclotron resonance physics relevant to an ECA measurement, drawing attention to those areas which may require further investigation to ensure a reliable interpretation of the measurements. Other plasma effects which may influence the measurement are discussed in Section 6.

2.1 Second Harmonic E-mode Optical Depth

The diagnostic will use the second harmonic E-mode since it has a suitable optical depth over most of the expected plasma parameter range, and since the only other possibility, the first harmonic O-mode, may suffer cut-off or significant refraction at the expected densities. The optical depth at the second harmonic E-mode resonance ($\omega = 2\omega_{ce}$) for quasi-perpendicular propagation in a Maxwellian plasma using the WKB approximation and lowest order finite Larmor radius formulations is given by [4]

$$\tau_2^E(n_e,T_e) = 2\pi^2 N^E \cdot (1 + A_2)^2 \cdot \{\frac{\omega_{pe}^2}{\omega_{ce}^2}\} \cdot \frac{T_e}{m_e c^2} \cdot \frac{L_B}{\lambda_o} \quad (1)$$

where λ_o is the vacuum wavelength, the E-mode index of refraction, N^E, is

$$N^E = \sqrt{1 - (\omega_{pe}^2/\omega_{ce}^2)\cdot(4\omega_{ce}^2-\omega_{pe}^2)/(3\omega_{ce}^2-\omega_{pe}^2)}, \quad (2)$$

$$A_2 = \frac{\omega_{pe}^2/\omega_{ce}^2}{2 \cdot (3 - \omega_{pe}^2/\omega_{ce}^2)} \quad (3)$$

and L_B is the scale length of the field inhomogeneity along the sightline, defined as

$$L_B = \left| \frac{B(s)}{dB/ds} \right| \quad (4)$$

where s is the length parameter along the sightline.

The tokamak toroidal magnetic field has a spatial dependence given approximately by

$$B(R) = \frac{B(R_o)\cdot R_o}{R} \quad (5)$$

so that

$$L_B = \frac{R}{\cos(\theta)} \quad (6)$$

where θ is the angle between the horizontal and the tangent vector to the sightline, and $B(R_o)$ is the field at R_o, the plasma centre. The poloidal magnetic field is neglected in the present analysis since it makes only a small contribution to the total field.

If the electron density is not too high ($n_e < 1.5\cdot10^{20}$ at B = 3 T) then the finite density terms (Equations 2 and 3) have an approximately linear density dependence, and the optical depth can be written as

$$\tau 2^E(ne,Te) \approx \frac{(1+\varepsilon n_e)\cdot n_e T_e}{31\cdot\cos(\theta)} \cdot \frac{R^2}{R_o^2} \qquad 10^{20} m^{-3} \cdot eV \quad (7)$$

where $\varepsilon = 2.7\cdot10^{-21}$ m^3.

The transmissivity $T(\omega)$ is given by

$$T(\omega) = \exp(-\tau_2^E). \quad (8)$$

2.2 Line Broadening Mechanisms

Using the usual expressions [5] for the relativistic ($\Delta\omega$rel) and Doppler ($\Delta\omega$dop) line widths and assuming a typical divertor T_e of 100 eV and R = 3 m, we obtain for the corresponding spatial widths:

$$\Delta R_{rel} = R \cdot \frac{\Delta\omega_{rel}}{\omega} \approx 2 \text{ mm} \quad (9)$$

$$\Delta R_{dop} = R \cdot \frac{\Delta\omega_{dop}}{\omega} \approx 2 \text{ mm for } \psi = 89.1° \quad (10)$$

where ψ is the angle between the ray direction and the magnetic field. Two aspects of the line broadening are worth noting because they are quite different to the situation normally encountered in the much hotter core plasma. First, Doppler broadening dominates unless the propagation is very close to perpendicular to the field. An accurate evaluation of the optical depth therefore requires that the propagation direction in relation to the field is well known. Secondly, the resonance layer width is about the same as the wavelength of the radiation.

2.3 Consequences of the Narrow Resonance Layer

The resonance layer thickness will be of the order of the radiation wavelength, λ_0. The theory of wave propagation through inhomogeneous plasmas and ECR absorption is based on the WKB approximation [4] which is violated in this case. Hence, full wave calculations are required to determine if the effects of other plasma processes are strong enough to influence the interpretation of the measurement. Reflection, mode conversion into electrostatic modes and polarization mixing at the resonant layer are possible sources of error for this measurement. In general, it is found that the transmitted power calculated using the WKB method and full wave methods agree [6], but that the resonant absorption is not necessarily equal to the loss in transmission, since the other effects also reduce the transmitted power. A full wave treatment of the second harmonic E-mode resonance phenomena for the low temperatures where the resonance feature is narrow and at densities appropriate to the JET divertor plasma is required.

3 INSTRUMENTAL ASPECTS OF THE ECA DIAGNOSTIC

3.1 Antennas and Waveguides

The access to the divertor region is very limited since the target tiles form an almost continuous surface, and are surrounded by the coils and cryopump. Moreover, any microwave components must be protected from the high heat fluxes in the divertor region. The solution we have adopted is to bring the waveguides through a bottom vertical port, to antennas located in the gap between the target tiles and recessed a few millimetres below the tile surface. The six antennas providing three sightlines are shown in Figure 2. Three antennas will be located in the centre of the divertor, two of them directed towards two antennas on the outboard side. The remaining centre antenna will point inwards to an inboard antenna. All of the antennas will be in one poloidal plane. The apertures of the antennas will be 7 mm in the toroidal direction (limited by the gap between the tiles) and ~15 mm in the poloidal plane. The separation between the antennas in each sightline is between 0.3 and 0.5 m. These parameters result in a low coupling efficiency, approximately -25 dB.

The waveguide from the torus to the diagnostic hall where the instrumentation will be located will be approximately 50 m long in each direction. It will make a number of horizontal and vertical turns to avoid existing structures (about 10 mitre bends) and pass under the biological shield. The waveguide will be oversized (S-band, WG10) to maximize the transmitted microwave power, and will incorporate a vacuum window interface at the torus and long tapers to change to smaller waveguide dimensions at each end. The overall attenuation expected is approximately 20 dB (10 dB in each direction).

All three microwave diagnostics (the interferometer and reflectometer in addition to the ECA system) will share this antenna and waveguide system. The ECA system can be multiplexed with the reflectometer and interferometer systems since they will operate in O-mode.

The characteristics of this antenna and waveguide system are important factors in choosing an ECA measurement technique. The large losses in the system place requirements on both the source power and receiver sensitivity. The options which have been considered are discussed in the following section.

3.2 Microwave Sources and Waveguide Effects

The internal dimensions (~50 mm) of the oversized waveguide used in the system are much larger than the radiation wavelength ($\lambda_0 \sim 2$ mm) and so many higher order modes can propagate. Discontinuities and imperfections in the waveguide can give rise to reflections, standing wave effects and mode conversion out of the TE_{01} and TE_{10} modes. The most important causes of these effects are the transition elements between straight sections of waveguide. These elements include 90° mitre bends in E or H-planes, tapers down to fundamental and near fundamental guide, vacuum windows and fundamental waveguide components (directional couplers, isolators, transitions, etc.). Every component can affect the power transmitted to the receiver. Figure 4 illustrates standing wave effects for a short section of straight guide bounded by 90° mitre bends. The waveguide section forms a resonant cavity of length L, producing multiple reflections (multi-passing) and a standing wave pattern in the electromagnetic field amplitude. If the field distribution within the cavity is disturbed (eg by dimensional changes in the waveguide or a change in source frequency), fluctuations in the power level at the receiver can be produced. Sources with a radiation coherence length less than the size of the components (i.e. incoherent radiation sources) do not give rise to standing wave effects.

Four possible instrumental techniques have been considered for the ECA diagnostic. A choice was made between them on the basis of the following requirements: a measurement of transmission over the 10-90% range to 10% accuracy (with SNR ~ 100:1), a spatial resolution of ~10 mm in major radius (1 GHz frequency resolution) and a measurement bandwidth of at least 10 Hz (and preferably much higher).

Incoherent Radiation Techniques

Two of the techniques involve incoherent radiation sources. The recirculated plasma light method consists of redirecting ECE from the core plasma, which is a bright source of thermal (incoherent) radiation, via a waveguide from the midplane to the ECA antenna system. The radiation is amplitude modulated and detected using a set of wideband heterodyne receivers and phase sensitive techniques to distinguish the recirculated emission from the background emission. To achieve the required signal to noise ratio, integration times ~10 s are necessary in order to overcome the strong background emission. Moreover, the system needs to be absolutely calibrated, in the same way as an ECE diagnostic. The expense, poor time resolution and limited accuracy due to calibration make this system an unattractive choice.

The source for the second method consists of a coherent radiation source and mode stirring to produce bright, incoherent radiation. This method is limited by the mechanical speed of the stirrer. The amplitude fluctuations in the radiation from a mode stirred cavity generate

an effective blackbody radiation bandwidth which is determined by the stirring method. Since this bandwidth is at most tens of kHz, integration times of seconds are required to achieve an adequate signal to noise ratio. For this reason the method was rejected. The mode stirred method has been used in laboratory experiments of microwave transmission [7], but considerably improved stirring techniques would be required for the present application.

Coherent Radiation Techniques

The other two techniques use coherent radiation sources directly. Both methods are based upon detecting the radiation having the minimum propagation time through the waveguide system and rejecting radiation which has experienced multi-passing. The pulsed source method incorporates high power, short pulse Impatt diodes sources and relies on discrimination in the time domain. The receiver is gated on only during the arrival of the first pulse and measures the energy content of this pulse. Coherence effects are not present for radiation pulses with lengths shorter than a given cavity dimension. Source power levels of one watt and pulse durations of one nanosecond can be obtained with these sources at frequencies up to 220 GHz. This method might be able to achieve the performance goals of the ECA instrument but was not an attractive choice on the basis of its high cost, complexity and requirement of a large number (~40) of Impatt sources to cover the frequency range.

The swept frequency method relies on discrimination in the frequency domain. A swept source is incorporated into an interferometer arrangement and the interference between the reference arm and plasma arm produces a beat at a frequency proportional to the difference in optical delay between the two arms and the rate of frequency sweep. With careful design of the system, a constant beat frequency can be produced at the receiver over the sweep period and the spurious beats (due to radiation multi-passing in the waveguide) will be displaced in frequency and can be rejected using a narrow band filter around the main beat frequency. The swept frequency system was chosen for its high measurement bandwidth, continuous coverage of the transmission profile and the availability of suitable microwave sources. The system is now described in detail.

3.3 Removal of Standing Wave Effects using the Swept Frequency Method

The method relies on a very linear sweep of the source frequency, which generates a constant beat frequency at the detector by interference between radiation from a fixed reference arm and that from the plasma arm. Radiation which experiences multiple reflections in the waveguide as it propagates to or from the plasma, and therefore may produce standing waves, travels a longer distance and generates a different beat frequency. The spurious or "ghost" beat frequencies can be excluded by filtering the output of the detector to a narrow range around the main beat frequency. This is illustrated in Figure 5.

The response time of the measurement is determined by the width of the filter which is used to discriminate against the ghost beat frequencies. To maximize this filter width, the source frequency must be swept as rapidly as possible. Similarly, the minimum distance between sources of reflection which can be excluded is also determined by the filter width since the closer together these reflectors are the closer the beat frequency generated is to the main single-pass beat.

If the rate of sweep of the source frequency is df/dt, and ΔL represents the difference in length between the plasma and reference arms, then the beat frequency is given by:

$$f_{beat} = df/dt \bullet \Delta L/c \quad (11)$$

since $\Delta L/c$ is the time delay between the two arms. A ghost beat generated by radiation having an extra propagation path around the system of δL will be separated from the main beat, at f_{main}, by

$$f_{ghost} = f_{main} + df/dt \bullet \delta L/c \quad (12)$$

The main beat frequency, due to single-pass radiation, will be amplitude modulated by variations in source power during the sweep, variations in transmission through the system, and by the plasma absorption. The amplitude modulation (AM) will give the line a non-zero width, as will the finite length of the sweep (i.e. the finite number of periods of the beat). With an estimate of this width, Equation 12 can be used to determine how linear the source frequency sweep must be in order that the whole of the broadened main beat always remains inside the filter pass-band, while all the ghost beats remain always outside the pass-band.

Equations 11 and 12 also show that if $\Delta L \sim \delta L$ then the ghost beat is relatively well spaced from the main beat. On the other hand, if ΔL is large (say, due to a very short reference arm) then the ghosts maintain the same absolute frequency separation from the main beat, but both main and ghost beats are much higher in frequency. In this latter case, the sweep must have much better linearity since any small deviations from linearity are magnified by the large ΔL, and the main beat could move outside the pass-band of the filter.

Not all standing wave effects will be eliminated by this technique: small components in the system, such as those in sections of fundamental waveguide, will produce ghosts within the pass-band of the filter. The design and construction of the system will have to be such that these residual ghosts are stable, so that their effect will be removed when the ratio is made of measurements with and without plasma.

4 THE ECA INSTRUMENT

A schematic of the ECA instrument is shown in Figure 6. The components in the schematic are described in detail in the subsequent sections.

4.1 Source and Detector

The sources, as shown in Figure 6, consist of two backward wave oscillators (BWOs) covering the frequency ranges: 118-178 GHz (WR-6 waveguide band) and 179-260 GHz (WR-4 waveguide band). These sources are capable of a full band sweep in one millisecond. Frequency sweeps of <35 GHz are sufficient to move the resonance from one antenna to the other. The frequency range from 120 to 260 GHz covers central magnetic field values between 2.3 and 3.4 T for the inboard and outboard sightlines. Output powers of 10 mW are expected from these sources. FM noise is an important source parameter for this application since ghost beats will have a noise bandwidth that can contribute energy within the frequency range used to reject ghosts. The FM noise of the BWO sources will be <-100 dBc/Hz, 100 kHz from the centre frequency.

An InSb hot electron bolometer will be used as a homodyne mixer. This detector was chosen for its wide spectral bandwidth, low NEP and high responsivity. The detector is limited

to an electrical signal bandwidth of 1 MHz. A solid state detector will be incorporated near the BWO source to monitor the source power over the sweep.

Assuming a frequency sweep of 30 GHz in 1 ms, and a difference in length between plasma and reference arms of ~1m, then a beat frequency of ~100 kHz will be generated. This is well within the bandwidth of the InSb detector, and permits a filter width around the beat frequency of ~50 kHz, while still excluding any ghost reflections with an additional path length due to multi-passing as short as 0.5m. However, it is then necessary to construct a reference arm of about the same length as the waveguide to and from the plasma.

4.2 Waveguide and Quasi-optical Reference Arm

The oversized waveguide arm has been designed so that all straight sections of guide have lengths greater than 1 m. The overall length of this arm is approximately 95 m. This spacing will place any ghost beats from these cavities outside the pass-band of the filter. Mode conversion has been minimized by using long non-linear tapers and using right angle mitre bends.

The reference arm will be of quasi-optical design, approximately one metre longer than the waveguide arm. A quasi-optical design was adopted for its high optical throughput, large spectral bandwidth and absence of waveguide discontinuities that would produce standing wave effects. To this end, the design uses focusing reflectors throughout. As shown in Figure 6, vertically polarized radiation from the source is split using a directional coupler into the waveguide and reference arm. The waveguide radiation transits the waveguide run and is launched in the quasi-optical system using a corrugated scalar horn. In the reference arm, the radiation is launched into a fundamental Gaussian beam mode using a corrugated scalar horn. The vertically polarized radiation passes through a polarizing grid, transits the 47.5 m to the roof mirror and retraces its path back to the grid. The roof mirror is tilted at 45° to vertical, so that the returning radiation is horizontally polarized. The return radiation is multiplexed with the waveguide radiation using a second polarizing grid. The two beams are focused onto the detector with an off-axis ellipsoidal mirror, after passing through an analysing grid to convert them into one polarization state.

4.3 Data Processing

A beat frequency signal in the 100 kHz range is suitable for real-time signal processing. During each plasma pulse, a sequence of sweeps will be generated, with dwell periods between them for processing the data. The properties of the system (ghost beats being displaced from the main beat to lower or higher frequencies) can be exploited and signal corrupting effects can be eliminated using real-time digital techniques in the time and frequency domain. Data processing will entail using a digital bandpass filter around the main beat, correcting the nonlinearities of the sweep to minimize frequency modulation of the beat, normalizing the detected power to a source monitor, using spectral techniques to eliminate corruptive effects in the signals from ghost beats, and reducing the amount of data to be stored. It will be possible to change the sweep characteristics during a plasma pulse in order to scan a much narrower range of frequencies or to operate in a single frequency mode.

5 THE ECA PROTOTYPE INSTRUMENT

A prototype ECA instrument has been assembled with the purpose of quantifying waveguide effects and demonstrating the technique. The layout of the apparatus is shown in Figure 7c. It is similar to the ECA instrumental layout in Figure 6. The mock-up consists of a 10 m quasi-optical reference arm, an 11 m oversized (S-band) waveguide with short tapers (< 1 m) and both E-plane and H-plane 90° mitre bends. To generate a strong ghost beat, a cavity was added to the waveguide arm. It consists of a non-polarizing beam splitter positioned at the junction of a straight waveguide section and the waveguide arm as shown. Mirrors were placed over the ends of the straight section and its length could be varied.

The source was a varactor tuned Gunn oscillator with a 6 GHz tuning range, from 86 to 92 GHz. The variation in output power over the sweep is shown in Figure 7a and can be seen in Figure 7b as amplitude modulation of the beat signal. The nonlinear voltage waveform required to produce a linear sweep is also shown in Figure 7a. The source frequency sweep was linearized by generating a tuning voltage waveform that positioned the zero crossings in the beat signal uniformly over the sweep time interval. To obtain a pure beat signal with no ghosts for this system, use was made of a parasitic interference beat which was found in the system. By rotating the roof mirror off the 45° position, an interference beat was found due to multi-passing in the quasi-optical system alone, the waveguide arm had been decoupled from the system. The frequency of this beat corresponded to a 10 m cavity length.

Figure 7b shows the results of the linearization process. An interferogram and its power spectrum are shown. The beat produced by the linearized source has high spectral purity, with sidebands suppressed to a level 35 dB below the main beat. A low level beat corresponding to a second pass through the 10 m reference arm is also present.

The beats from the complete system do not have such high spectral purity as the beats produced from the reference arm alone, since the waveguide used for these experiments has some discontinuities and imperfections. For example, short tapers (< 1 m) were used from fundamental guide to S-band guide. Two power spectra of the interference signal for the complete system with both arms beating is shown in Figure 7d. The main beat is broader than that in Figure 7b, due to standing wave effects in the waveguide. The ghost beat which is visible is caused by the cavity that was introduced into the oversized waveguide. The frequency difference between the main beat and the ghost can be varied as shown in Figure 7d by changing the length of the cavity. The change in frequency of the ghost is exactly as expected from Equation 11 and the change in cavity length. No other strong lines in the power spectrum are observed in this system over the 6 GHz frequency sweep suggesting that subsidiary standing wave effects in this experiment are weak.

6 COMPENSATION FOR NON-ECA LOSSES

The principal problem in the interpretation of the measurements will be due to the changes in the transmitted signal power which are caused by effects other than ECA. Several effects need to be considered. They can be summarized in the following simple equation for the power fraction transmitted through the plasma:

$$T = 1 - A - R_a - S - R_e - M \pm P \qquad (13)$$

where A represents the resonant absorption, R_a is the power loss due to refraction distorting the transmitted beam, S is the fraction of the power scattered by density fluctuations, R_e and M represent the power reflected and mode converted at the resonance layer, and P accounts for polarization mixing which may reduce or increase the received power.

6.1 Refraction

Refraction can be considered as a time dependent coupling between the antennas. The small antennas will produce radiation patterns with 24° to 40° FWHM. For this reason, the coupling between the antennas should not be too sensitive to refractive effects. However, provision will be made to correct for refraction by extending the frequency sweep beyond the resonance range of frequencies between the antennas, the attenuation at these frequencies being due solely to the refraction, which is generally only weakly dependent on frequency.

Another problem will be the precise determination of the location of the resonant absorption in the divertor region. Numerical modelling is being used to simulate refractive effects using ray tracing. Magnetic equilibria for the future pumped divertor plasmas have been calculated and density and temperature profiles based on probe measurements in X-point plasmas are used.

6.2 Scattering, Mode conversion and Reflection

Scattering of the radiation may be caused by density fluctuations (plasma turbulence) in the divertor region. The effect of scattering should be an attenuation of the radiation which is only weakly frequency dependent. This is similar to refraction and the same method of compensation should be applicable. The effects of reflection and mode conversion at the resonance layer were mentioned in Section 2.3. For low temperature plasmas (~10 eV) losses of the order of a few percent might be expected from resonant reflection and resonant mode conversion. Full wave calculations of these effects at the second harmonic E-mode resonance in this low temperature, high density plasma regime are in progress [8].

6.3 Polarization Mixing

Due to access limitations, the antennas will launch and receive radiation which is polarized with the E-vector in the poloidal plane (ie. quasi-vertical polarization). However, the magnetic field lines will be slightly tilted from the horizontal (in order to intercept the divertor target at a shallow angle), so a small fraction of the power will be launched as O-mode. Since the second harmonic O-mode optical depth will be very low, this radiation will be only weakly attenuated and some of it will couple into the receive antenna in the vertical polarization. Although this effect will be small, it may be significant at the two extremes of the E-mode optical depth range. When the E-mode optical depth is large, the excess received power (which passed through the plasma as O-mode) will produce a lower apparent absorption for the E-mode. On the other hand, when the E-mode optical depth is small, the loss of power into the O-mode will give an apparent increase in the E-mode absorption.

For the magnetic configurations under study, the launch polarization can be up to 2° from pure E-mode. The field angle will be measured near the antennas by the magnetic

diagnostics in the divertor and a knowledge of the magnetic equilibrium may allow us to correct the data for this effect.

7 CONCLUSIONS

Experimental evidence suggests that the underlying physics of ECA is well enough understood, at least for the usual tokamak operating conditions, to use ECA as a routine diagnostic. For second harmonic E-mode and first harmonic O-mode the optical depth at modest density is proportional to the electron pressure or neTe product and for the JET divertor plasma the level of absorption expected lies within the detection limits of a well designed microwave absorption diagnostic. The measurement will be susceptible to spurious changes in transmitted power, predominantly due to the coherent radiation sources generating standing waves in the oversized and complex waveguides. However, with careful design of the waveguide transmission system and the method of detection, these effects can be removed from the measurement.

The chosen method is a swept frequency system and a prototype of the instrument has shown the expected standing wave effects are present but can be removed. This process will be continued through to the final system.

Plasma effects or non-ECA inputs such as refraction and polarization mixing can be eliminated in practice by sweeping the resonance beyond the antennas and using magnetic equilibria as an input in the interpretation of the data. Plasma effects around the resonance layer such as reflection and mode conversion to Bernstein electrostatic modes need to be quantitatively studied for this plasma regime.

8 ACKNOWLEDGEMENTS

The authors wish to thank Drs Jim Lesurf and Andy Harvey of the University of St. Andrews for stimulating discussions on the swept frequency method, and wish to thank Dr Richard Wylde of Thomas Keating Ltd, for contributions to the design of the prototype quasi-optical reference arm.

9 REFERENCES

[1] Huguet M et al., 14th Symposium on Fusion Engineering (San Diego, 1991)

[2] Pachtmann A, Wolfe S M and Hutchinson I H, Nucl. Fusion, **30** (8), 1283 (1987)

[3] Kirkwood R K, Hutchinson I H, Luckhardt S C, Squire J P, Nucl Fusion, **30**(3), 431 1990)

[4] Bornatici M. et al., Nucl. Fusion, **23**(9), 1153 (1983)

[5] Engelmann, F., Curatolo M., Nucl. Fusion, **13**, 497 (1973)

[6] Imre, K, Weitzner, H, Phys Fluids, 28 (1), 133 (1985)

[7] Birch J R, Bechtold G, Kremer F, Poglitsch A, NPL Report DES 79 (1983)

[8] Lashmore-Davies C N, Private Communication

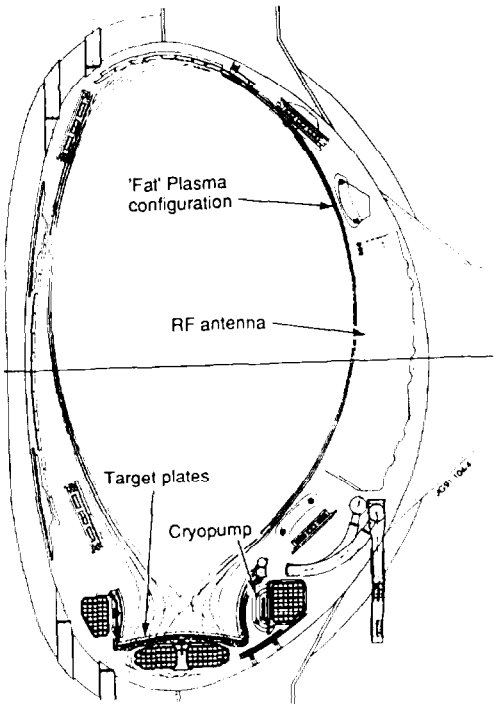

Figure 1: A poloidal cross-section of JET showing the pumped divertor target plates, coils and cryopump. Calculated flux surface in the scrape-off layer for a "fat" plasma configuration are also shown.

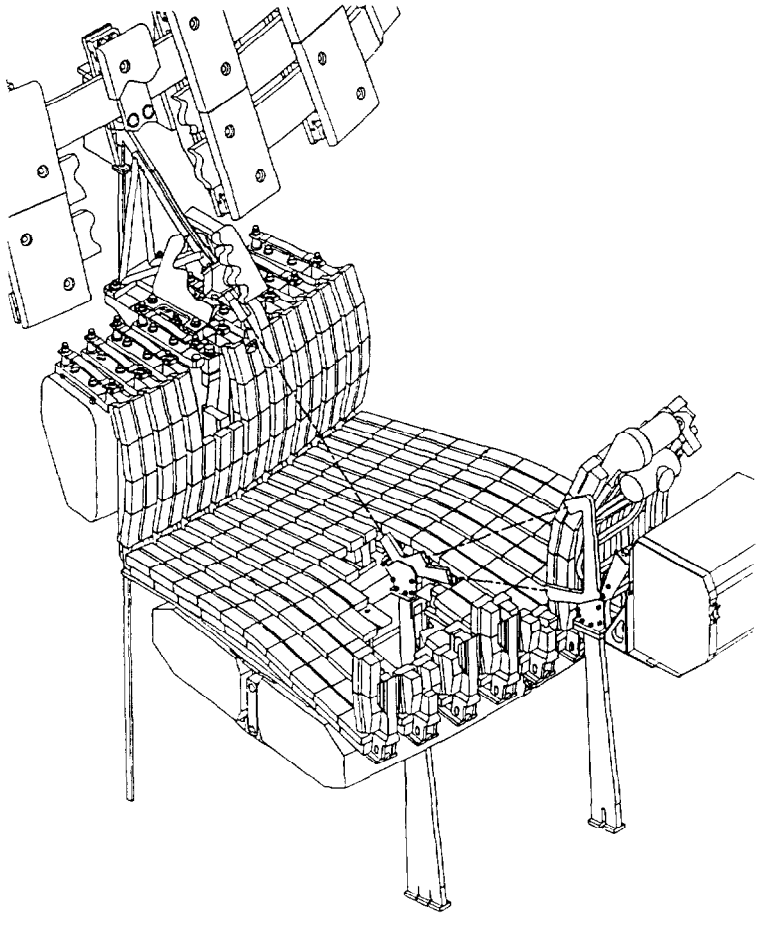

Figure 2: A three-dimensional sketch of a section of the divertor target plates, showing the locations of the ECA antennas. The three antennas in the centre provide two sightlines to the outboard side and one to the inboard side.

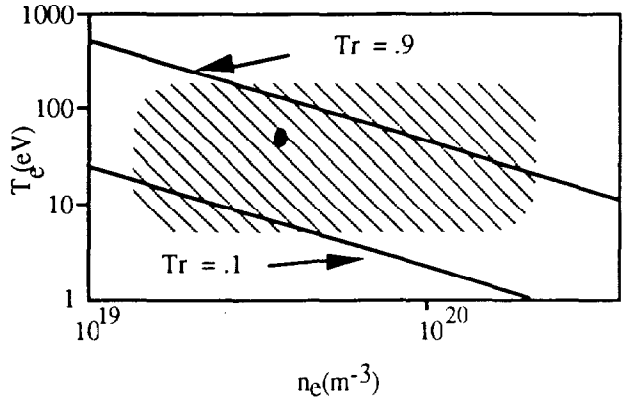

Figure 3: (n_e,T_e) diagram showing microwave transmission (Tr) in relation to the divertor plasma's parameter space. The .1 and .9 levels of transmission are shown.

\\\ expected divertor plasma operating regime

• a likely operating point (70 eV, $4 \cdot 10^{19}$)

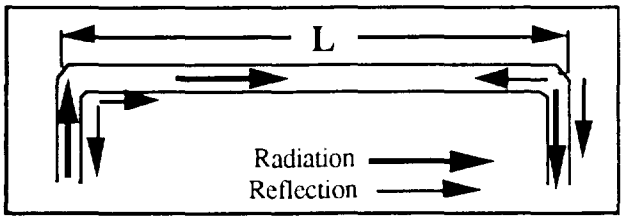

Figure 4: A straight section of oversized waveguide bounded by 90 degree mitre bends. Reflections at the ends will cause standing wave effects and delayed signals to appear at the receiver.

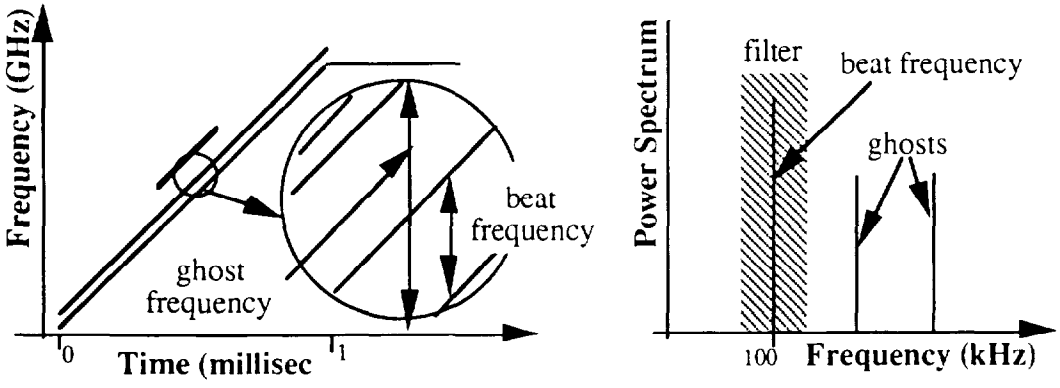

Figure 5: Frequency vs time for the reference arm radiation, waveguide arm radiation and echoes. The mixing at the detector produces a series of beats in frequency, the lowest frequency being the interference between the reference arm radiation and the waveguide radiation with minimum delay.

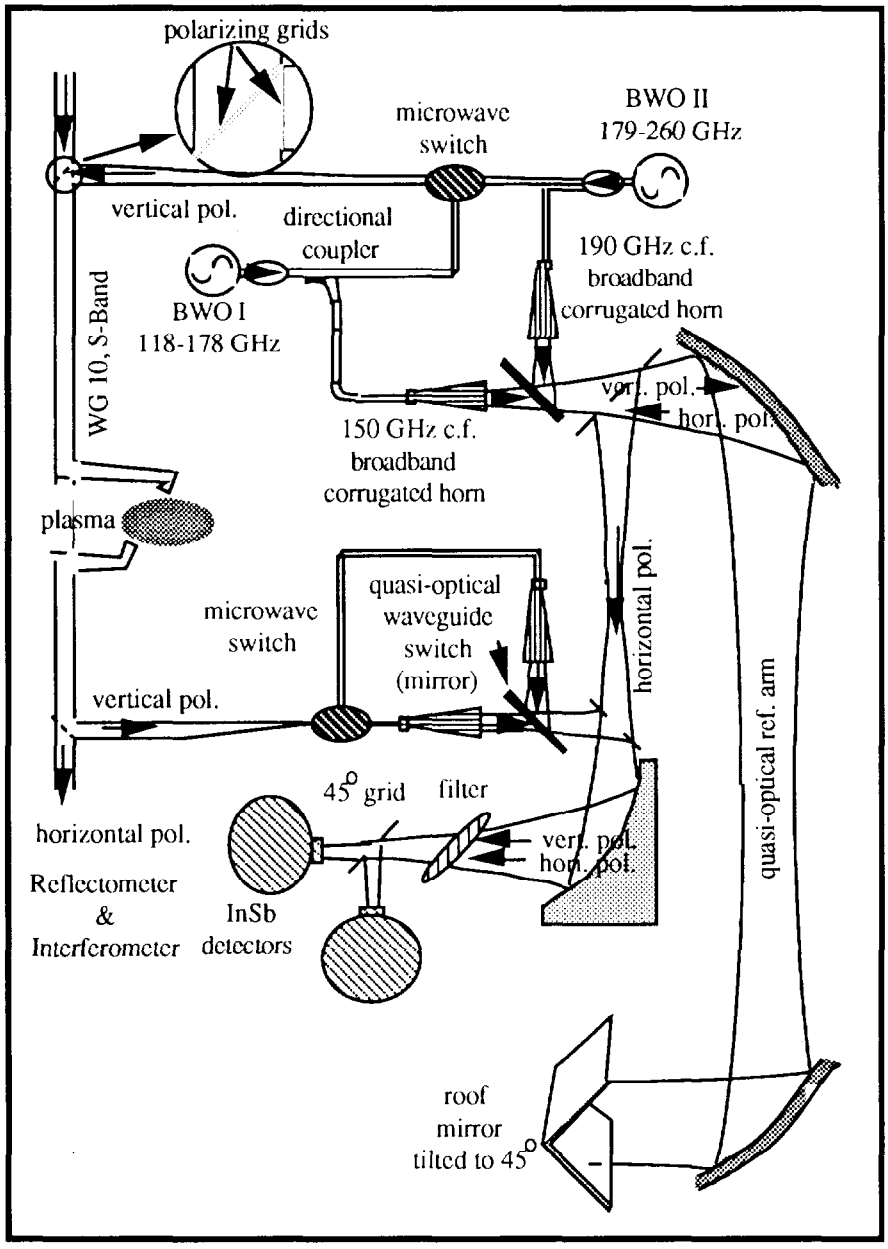

Figure 6: ECA instrumental layout. The 120-240 GHz frequency range is covered by two BWO sources in two waveguide bands (WR4 and WR6). The radiation is multiplexed in oversized waveguide using polarising grids. The other diagnostics sharing the waveguide use O-mode polarisation.

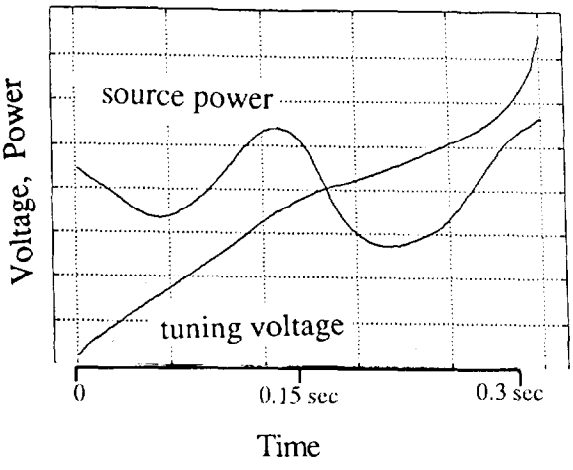

Figure 7a: Output power and varactor tuning voltage for a sweep (arb. scale).

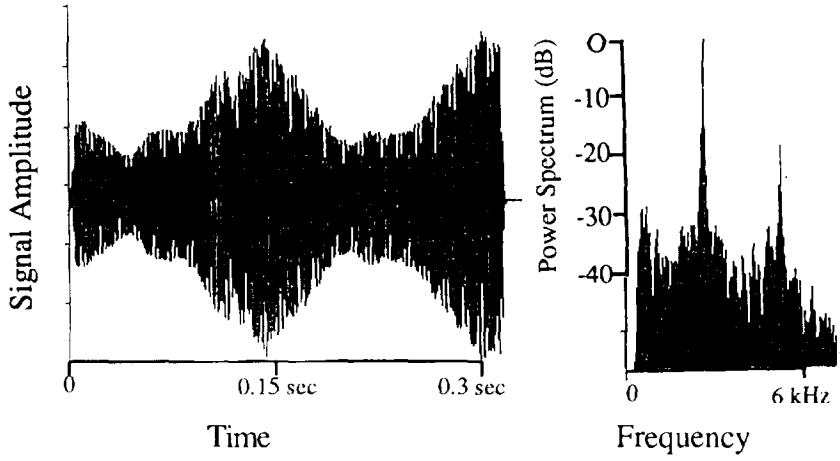

Figure 7b: Interferogram of quasi-optical ref. arm with a linearised source and its power spectrum (log scale).

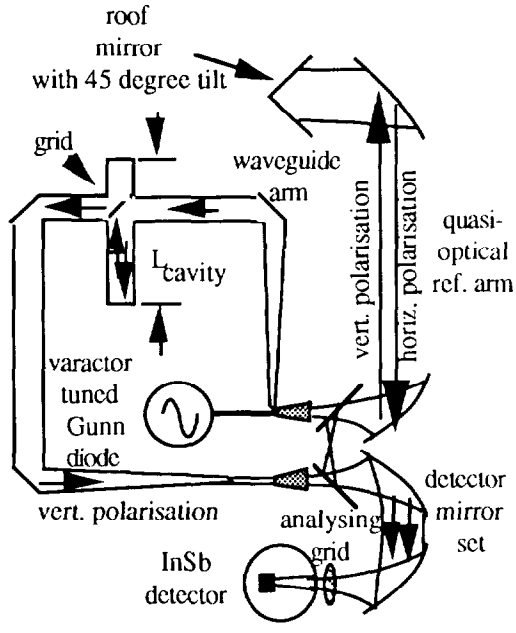

Figure 7c: Layout of ECA mock-up instrument.

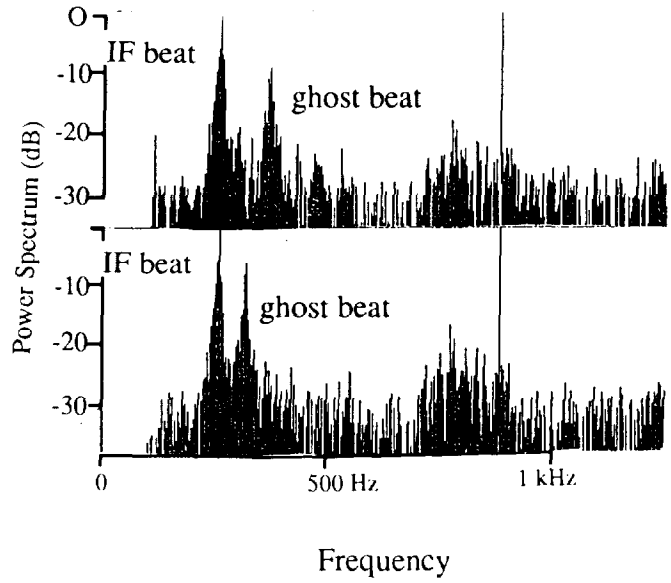

Figure 7d: Power spectra of beat interferograms between ref. arm and waveguide arm, cavity length is varied (log scale).